Spin Hall magnetoresistive detection of easy-plane magnetic order in the van der Waals antiferromagnet math xmlns="http://www.w3.org/1998/Math/MathML">msub>mi >NiPS/mi>mn>3/mn>/msub>/math>

Kohki Sugi, Takuto Ishikawa, Motoi Kimata, Yoichi Shiota, Teruo Ono, Takeo Kato, and Takahiro Moriyama

Phys. Rev. B **108**, 064434 — Published 31 August 2023

DOI: 10.1103/PhysRevB.108.064434

Spin Hall magnetoresistive detection of the easy-plane magnetic order in van der Waals antiferromagnet $NiPS_3$

Kohki Sugi[1], Takuto Ishikawa[2], Motoi Kimata[3], Yoichi Shiota[1,4], Teruo Ono[1,4],

Takeo Kato[2], Takahiro Moriyama[†] [5,6]

[1] Institute for Chemical Research, Kyoto University, Uji, Kyoto, 611-0011, Japan.

[2]The Institute for Solid State Physics, The University of Tokyo, Kashiwa, Chiba, 277-8581, Japan

[3] Institute for Materials Research, Tohoku University, Sendai, Miyagi, 980-8577, Japan

[4] Center for Spintronics Research Network, Kyoto University, Uji, Kyoto 611-0011, Japan

[5] Department of Materials Physics, Nagoya University, Nagoya, Aichi, 464-8603, Japan

[6] PRESTO, Japan Science and Technology Agency, Kawaguchi, Saitama 322-0012, Japan

Abstract

Magnetic van der Waals materials offer a new physical paradigm for studying 2-dimensional (2D) magnetic systems. 2D antiferromagnets are of great interest in the emerging field of antiferromagnetic spintronics where interaction between local antiferromagnetic moments and a spin current is fully utilized. Here, we report the spin Hall magnetoresistance (SMR) in the $NiPS_3$/Pt system. The magnetic field and temperature dependence of the resistivity change unambiguously revealed the magnetic properties of $NiPS_3$, such as the easy-plane anisotropy and the Neel temperature. As SMR is a manifestation of the magnetic moments interacting with the spin current that is an essential requirement in spintronics, our results open an avenue for 2D antiferromagnetic spintronics.

[†] Corresponding to: moriyama.takahiro.a4@f.mail.nagoya-u.ac.jp

Antiferromagnetic spintronics has been one of the emerging topics in the field of spintronics[1,2]. Recent vigorous investigations have revealed a variety of spintronic phenomena with antiferromagnets such as magnetoresistance[3,4], spin torque effect[5,6,7,8,9], and spin current transmission[10,11,12,13], THz spin pumping effect[14,15,16]. These observations confirm that there exist interactions between spin currents and the localized magnetic moments in antiferromagnets which are essential for operation principles for modern spintronic devices. Antiferromagnetic spintronics offers a wide range of material choices in spintronic applications since antiferromagnetic materials are abundant comparing to ferromagnetic ones. Recent explorations cover a wide variety of materials, such as transition metal oxide (NiO, CoO, etc.) and metallic alloy (MnIr, MnSn, etc.), having collinear and non-collinear 3-dimensional antiferromagnetic order. However, interaction between spin current and van der Waals antiferromagnets with 2-dimensional antiferromagnetic order has not been explored as much except few examples such as $FePS_3$/Pt[17] and $CrPS_4$/Pt[18].

Nickel phosphorus trisulfide, $NiPS_3$, is one of the layered transition metal thiophosphates, MPS_3 (M = Mn, Fe , Ni etc.), where the transition metal atoms make layers of honeycomb lattice in the *a*-*b* plane and the layers are weakly bonded each other by van der Waals force. It is an antiferromagnetic insulator with a bandgap of ~1.6 eV[19]. As shown in Fig. 1, below the Neel temperature (T_N = 155 K), spins on Ni cation form a 2-dimensional antiferromagnetic order. $NiPS_3$ has an easy-plane magnetic anisotropy in the *a*-*b* plane[20] which is distinct from majorities of the MPS_3 family having magnetic anisotropy perpendicular to the *a*-*b* plane[21]. There is a three-fold axial magnetic anisotropy due to the honeycomb symmetry of the *a*-*b* plane. $NiPS_3$ is often referred to as a model material for the XY spin system[22] which could lead to the magnetic analogue of the quantum fluid relevant to the spin superfluidity[23]. It is interesting to note that the magnetic susceptibility peaks at temperature (~300 K) much higher than T_N which is significantly distinct from conventional 3-dimensional antiferromagnets[22].

The spin Hall magnetoresistance (SMR) has been found useful to probe the interaction between spin current and the localized magnetic moments in variety of magnetic materials including antiferromagnets[24,25,26,27,28]. SMR emerges in a multilayer having an interface between a magnetic material and a spin Hall material (such as Pt, Ta, W, etc.). As it can sense the magnetic moments at the interface, it is possible to probe the van der Waals magnets down to monolayer limit. The SMR essentially originates from the interaction of $\mathbf{m}_i \cdot \boldsymbol{\sigma}$ where $\boldsymbol{\sigma}$ is a unit vector representing the spin polarization created by the spin Hall material and $\mathbf{m}_i$ is a unit vector representing the localized microscopic magnetic moment[29,30]. Since the spin Hall effect yields $\boldsymbol{\sigma}$ orthogonal to the direction of the electrical current flow $\mathbf{I}$, the SMR shows a characteristic dependence on the relative orientation of $\mathbf{I}$ and $\mathbf{m}_i$. A fundamental expression of the SMR in a resistivity ρ is given as,

$$\rho = \rho_0 + \Delta\rho_{SMR} \frac{1}{N} \sum_{i=1}^{N} [1 - (\mathbf{m}_i \cdot \boldsymbol{\sigma})^2]. \tag{1}$$

where ρ_0 is the resistivity irrelevant to the SMR, N is the total number of the localized magnetic moments, and $\Delta\rho_{SMR}$ is a coefficient representing a full resistivity change due to the SMR.

For collinear antiferromagnets with two magnetic sublattices below T_{N}, the resistivity ρ varies due to the SMR as,

$$\rho = \rho_0 + \Delta\rho_{SMR}[1 - (\mathbf{m}_1 \cdot \boldsymbol{\sigma})^2/2 - (\mathbf{m}_2 \cdot \boldsymbol{\sigma})^2/2], \tag{2}$$

where $\mathbf{m}_{1,2}$ is the magnetic moment of the each sublattice. As we introduce the Neel vector $\mathbf{N} = (\mathbf{m_1} - \mathbf{m_2})/2$ and the magnetization vector $\mathbf{M} = (\mathbf{m_1} + \mathbf{m_2})/2$, Eq. 1 can be rewritten as,

$$\rho = \rho_0 + \Delta\rho_{SMR}[1 - (\mathbf{N} \cdot \boldsymbol{\sigma})^2 - (\mathbf{M} \cdot \boldsymbol{\sigma})^2]. \quad (3)$$

In a spin-flop phase with a sufficiently large external magnetic field $\mathbf{H}$, $\mathbf{M}$ and $\mathbf{N}$ respectively become parallel to and perpendicular to $\mathbf{H}$. While there have been reports on the SMR study with van der Waals antiferromagnet $FePS_3$ and $CrPS_4$ with $\mathbf{m}_i$ pointing out of the plane in the ground state[17,18], $NiPS_3$ with $\mathbf{m}_i$ laying in the plane gives rise to a different SMR signature as a function of the field direction as well as the strength. Moreover, in the paramagnetic phase above T_N, $\mathbf{m}_i$ favors to point in the direction of $\mathbf{H}$. Therefore, by looking into ρ with respect to $\mathbf{H}$, one can investigate the magnetic order and the phase transition in antiferromagnets.

In this paper, we explore the magnetic order and its temperature dependence in $NiPS_3$/Pt multilayer by the SMR. The SMR was characterized by magneto-transport measurements performed at elevated temperatures with an external magnetic field rotating in the *a-b* plane. The field angle dependence of the SMR was found consistent with the easy-plane antiferromagnetic order in $NiPS_3$. The temperature dependence of the SMR allows us to determine T_N and shows an intriguing manifestation relevant to the 2-dimensinality of the magnetic order.

$NiPS_3$ flakes are mechanically exfoliated from a bulk single crystal (with the purity $\geq$ 99.999%) by a strip of adhesive tape. In order to avoid any possible oxidation and contamination on the surface, we transfer the flakes on a thermally oxidized Si substrate in a vacuum chamber with the base pressure of 10^{-5} Pa and subsequently deposit 5 nm-thick Pt layer by a d.c. magnetron sputtering. Pt electrode patterns and Au/Ti leads for resistance measurement are fabricated by conventional electron beam lithography and

Ar ion milling process. The magneto-transport measurements were performed with dc 4-probe measurement in the temperature range of 10 to 300 K by using the cryocooled superconducting magnet (25T-CSM) in the High field Laboratory for Superconducting Materials, Tohoku University, which can generate a static field up to 24 Tesla. The measurement configuration is defined with respect to the electric current $\mathbf{I}$ flowing in *x* axis as shown in Fig. 1 (b), where the *x*-*y* plane is set parallel to the *a*-*b* plane of $NiPS_3$. The external magnetic field $\mathbf{H}$ rotates within the *x*-*y* plane with the angle φ relative to the *x* axis. Presuming the easy-plane magnetic anisotropy, sublattice magnetic moments $\mathbf{m}_1$ and $\mathbf{m}_2$ of the $NiPS_3$ (see Figs. 1(a) and (b)) can only rotate in the *a*-*b* plane. Therefore, when it undergoes a spin-flop state in the antiferromagnetic phase, $\mathbf{m}_1$ and $\mathbf{m}_2$ become nearly perpendicular to $\mathbf{H}$ within the *x*-*y* plane. The Neel vector $\mathbf{N}$ and the magnetization vector $\mathbf{M}$ are also depicted in Fig. 1 (b). For the antiferromagnetic phase, considering $\mathbf{N} \perp \mathbf{H}$, $\mathbf{M} \parallel \mathbf{H}$ and $|\mathbf{N}|^2 + |\mathbf{M}|^2 = 1$, we can rewrite Eq. 3 for our measurement setup as,

$$\rho = \rho_0 + \Delta\rho_{SMR}[|\mathbf{N}|^2 \sin^2\varphi + |\mathbf{M}|^2 \cos^2\varphi]. \tag{4}$$

By taking φ dependence of ρ, one can identify the magnetic phase transition as well as determine which of $\mathbf{N}$ or $\mathbf{M}$ is dominant in the antiferromagnetic phase.

Main results shown in this paper are from the devices shown in Figs. 1 (c) and (d) which are labeled as dev#1 and dev#2, respectively. Thickness of $NiPS_3$ was measured to be 210 nm and 142 nm for dev#1 and dev#2, respectively, by atomic force microscopy. The dimensionless magnetic susceptibility χ of a bulk single crystal $NiPS_3$, from which the flakes are exfoliated, was characterized along the crystalline axes by SQUID magnetometer.

Figure 2 shows the change of resistivity $\Delta\rho/\rho_0$ as a function of φ with various

$\mu_0|\mathbf{H}|$ up to 24 Tesla at 10 K. Both devices show the development of the $\sin^2\varphi$ profile with increasing the magnetic field, suggesting that $\mathbf{N}\perp\mathbf{H}$ and $\mathbf{N}$ predominantly rotates in the *a*-*b* plane, *i.e.* the easy-plane. The results therefore indicate that the $NiPS_3$ flakes are in antiferromagnetic phase at T = 10 K. The maximum $\Delta\rho/\rho_0$ at 24 T is in the order of 10^{-4} for both devices, which is comparable to those observed in various magnet/Pt systems[24,25,26,27,29] . Figure 3 shows $\Delta\rho/\rho_0$ as a function of φ at various temperatures with $\mu_0|\mathbf{H}|$ = 24 Tesla. As the temperature increases up to 300 K, for both devices, the $\sin^2\varphi$ profile gradually becomes the $\cos^2\varphi$ profile, suggesting $\mathbf{M}\parallel\mathbf{H}$ and $\mathbf{M}$ becomes dominant at high temperature (see Eq. 4) and therefore indicating that the $NiPS_3$ undergoes the antiferromagnetic-paramagnetic phase transition. The observed SMR behaviors are over all consistent with the known magnetic properties of $NiPS_3$.

We now discuss in detail over the temperature and field dependence of $\Delta\rho_{max}/\rho_0$, where $\Delta\rho_{max}/\rho_0$ is the maximum magnetoresistance ratio obtained by fitting the data presented in Figs. 2 and 3 with $\frac{\Delta\rho_{max}}{\rho_0}\cos^2\varphi$. We note that $\Delta\rho_{max}/\rho_0$ is therefore positive when $\mathbf{M}$ is dominant in the paramagnetic phase and negative when $\mathbf{N}$ is dominant in the antiferromagnetic phase.

First, we look into the field dependence of $\Delta\rho_{max}/\rho_0$ shown in Fig. 4. The quadradic field dependence, which is well fitted by $k(\mu_0 H)^2$ with a constant k, indicates that the spin-flop phase is not driven by a coherent rotation of $\mathbf{N}$ with a single domain state but driven by a magnetic domain redistribution with a multidomain state[31]. Since the magnetic axial anisotropy within the *a*-*b* plane can be a 3-fold degeneracy due to the six-fold rotational symmetry in the honeycomb lattice, it is very natural for $NiPS_3$ to be in a multidomain state with the three possible magnetic domains within which $\mathbf{N}$ points in one of the three magnetic easy axes quite similarly to the case for NiO[31].

Therefore, multidomain state of the $NiPS_3$ is a quite reasonable account.

Second, we analyze the temperature dependence of $\Delta\rho_{max}/\rho_0$ and the dimensionless magnetic susceptibility χ shown in Fig. 5. $\chi_{\|a}$, $\chi_{\|b}$, and $\chi_{\|c*}$ are respectively the magnetic susceptibilities along the crystalline axis a, b, and c* which is perpendicular to the a-b plane and $c \neq c^*$. It is clearly seen that the temperature at which $\Delta\rho_{max}/\rho_0$ becomes zero is ~ 155 K which corresponds well to the reported Neel temperature of $NiPS_3$ and to the temperature at which $\chi_{\|a}$, $\chi_{\|b}$, and $\chi_{\|c*}$ are all merged. Above T_N, $\Delta\rho_{max}/\rho_0$ is positive and shows a plateau around 260 K. This plateau resembles the temperature dependence of the magnetic susceptibility of $NiPS_3$ (Fig. 5 (b)) that is considered to be associated with the 2-dimensional nature of the magnetism[20]. On the other hand, below T_N, $\Delta\rho_{max}/\rho_0$ is negative and increases with increasing temperature in a different manner than any of $\chi_{\|a}$, $\chi_{\|b}$, or $\chi_{\|c*}$. The power law analysis reveals that $\Delta\rho_{max}/\rho_0$ scales with $(T_N - T)^{0.9}$ (see the inset of Fig. 5), which is quite distinct from $(T_N - T)^{0.7}$ of the conventional 3-dimensional antiferromagnets[24,28] and could reflects the characteristic of 2-dimensional antiferromagnetic order at the Pt/ $NiPS_3$ interface.

Next, we relate the SMR with the spin mixing conductance $g_{\uparrow\downarrow}$ at the Pt/ $NiPS_3$ interface. The full SMR ratio $\Delta\rho_{SMR}/\rho_0$ is known to be governed by[30],

$$\frac{\Delta\rho_{SMR}}{\rho_0} = \theta_{SH}^2 \frac{\lambda}{d_{Pt}} \left(\frac{2\lambda g_{\uparrow\downarrow} \tanh^2 \frac{d_{Pt}}{2\lambda}}{\sigma_{Pt} + 2\lambda g_{\uparrow\downarrow} \coth \frac{d_{Pt}}{\lambda}} \right) \tag{5}$$

where θ_{SH}, λ, d_{Pt}, and σ_{Pt} are the spin Hall angle, the spin diffusion length, the thickness, and the conductivity of Pt. Since the $NiPS_3$ is found to be multidomain below T_N, our maximum field 24 Tesla does not seem to saturate $\Delta\rho_{max}/\rho_0$, *i.e.* $\Delta\rho_{max}/\rho_0 \neq \Delta\rho_{SMR}/\rho_0$. In this situation, we need to multiply a factor $(H/H_{MD})^2$ to the r.h.s of Eq.

5, where H_{MD} is a monodomainizaion field at which the domains merge into a monodomain [31]. While it is not possible to experimentally apply large enough field to saturate the domain and to determine H_{MD}, we estimate the spin mixing conductance normalized by H_{MD} as $g_{\uparrow\downarrow}(24\ \mathrm{T}/\mu_0 H_{MD})^2$ =7.8 x 10^{12} Ω^{-1} m^{-2} using θ_{SH}= 0.12, λ = 3 nm [32], d_{Pt} = 5nm and the measured value of σ_{Pt} = 1.3 x 10^6 Ω^{-1} m^{-1}. We should note that the contribution of the Henle magnetoresistance (HMR)[33], which has a similar symmetry with respect to the field angle φ, is not subtracted from $\Delta\rho_{max}/\rho_0$. It has been known that, depending on the quality of Pt film, the underlayers, and so on[33], HMR is sometimes significant enough to complicate the precise SMR analysis especially at high field. If any, HMR gives rise to resistance change as a function of $\cos^2\varphi$ therefore adds a positive contribution to $\Delta\rho_{max}/\rho_0$, leading to underestimation of $g_{\uparrow\downarrow}(24\ \mathrm{T}/\mu_0 H_{MD})^2$. Nevertheless, our observation that $\Delta\rho_{max}/\rho_0$ becomes completely zero in close vicinity of the Neel temperature (Fig. 5(a)) suggests that the contribution of HMR is negligible in our sample.

Finally, let us discuss the temperature dependence of $\Delta\rho_{max}/\rho_0$. By the microscopic theory [34], the SMR ratio is written by a sum of two contributions as $\Delta\rho_{max}/\rho_0 \propto \tilde{\rho}_1 + \tilde{\rho}_2$, where $\tilde{\rho}_1$ is a static part determined only by the sublattice magnetizations, $\mathbf{m}_1$ and $\mathbf{m}_2$, as discussed above, and $\tilde{\rho}_2$ is a dynamic part due to annihilation and creation of magnons [35]. The temperature dependence of the former contribution obtained by the mean-field approximation is shown by the blue solid line in Fig. 5 (a). This result captures the qualitative feature of SMR; it approaches zero in the vicinity of the Neel temperature T_N = 155 K. We note that zero SMR at a high temperature is false as the mean field calculation cannot take into account the paramagnetic spin polarization above the Neel temperature. The dynamic contribution can be calculated as a correction to the static one by the magnon dispersion at low temperature. The sum of the two contributions is also shown by the green solid line in Fig. 5 (a) which fits better than the blue solid line, indicating that the dynamic contribution is quite important to interpret the SMR in this system.

In summary, we investigated the spin Hall magnetoresistance in the $NiPS_3$/Pt system in the rotating magnetic field. The magnetic field and temperature dependence of the resistivity change are well understood by the framework of the spin Hall magnetoresistance with the magnetic properties of $NiPS_3$, such as the easy-plane anisotropy and the Neel temperature. Moreover, the temperature dependence of the SMR in the antiferromagnetic phase is well reproduced by the microscopic SMR theory including the magnon contributions. As SMR is a manifestation of the interaction of the spin current and the magnetic moments of the $NiPS_3$ via the interface, our results essentially suggest that the various spintronic operation principles, such as spin torque and spin pumping, involving the spin current would be effective on this van der Waals antiferromagnet. Our results therefore open an avenue for 2D antiferromagnetic spintronics.

Acknowledgements

This work was supported in part by JSPS KAKENHI Grant Numbers JP21H04562, JP21H05470, JP20H05665, JP20K03831 and JST PRESTO Grant Number JPMJPR20B9. The experiments were performed at the High Field Laboratory for Superconducting Materials, Institute for Materials Research, Tohoku University (Project No 202112-

HMKPD-0056). T. I. is supported by International Graduate Program of Innovation for Intelligent World (IIW) of The University of Tokyo.

Figure captions:

Fig. 1 (a) Schematic illustration of the crystalline and magnetic structure of $NiPS_3$. (b) The measurement configuration of the applied magnetic field. The optical microscope images of (c) the device #1 and (d) the device #2.

Fig. 2 $\Delta\rho/\rho_0$ as a function of the field angle φ with various field magnitude $\mu_0 H$ at T = 10 K.

Fig. 3 $\Delta\rho/\rho_0$ as a function of the field angle φ at elevated temperature with $\mu_0 H$ = 24 T.

Fig. 4 Field dependence of $\Delta\rho_{max}/\rho_0$ at T = 10 K.

Fig. 5 (a) Temperature dependence of $\Delta\rho_{max}/\rho_0$ with $\mu_0 H$ = 24 T. The inset is a log-log plot of $|\Delta\rho_{max}/\rho_0|$ with (T_N - T) as a horizontal axis. The green and blue lines are derived by the microscopic SMR theory with and without magnon contributions, respectively. Dotted lines indicate a regime where the microscopic theory is inappropriate due to various approximations. (b) Temperature dependence of the dimensionless magnetic susceptibility of $NiPS_3$.

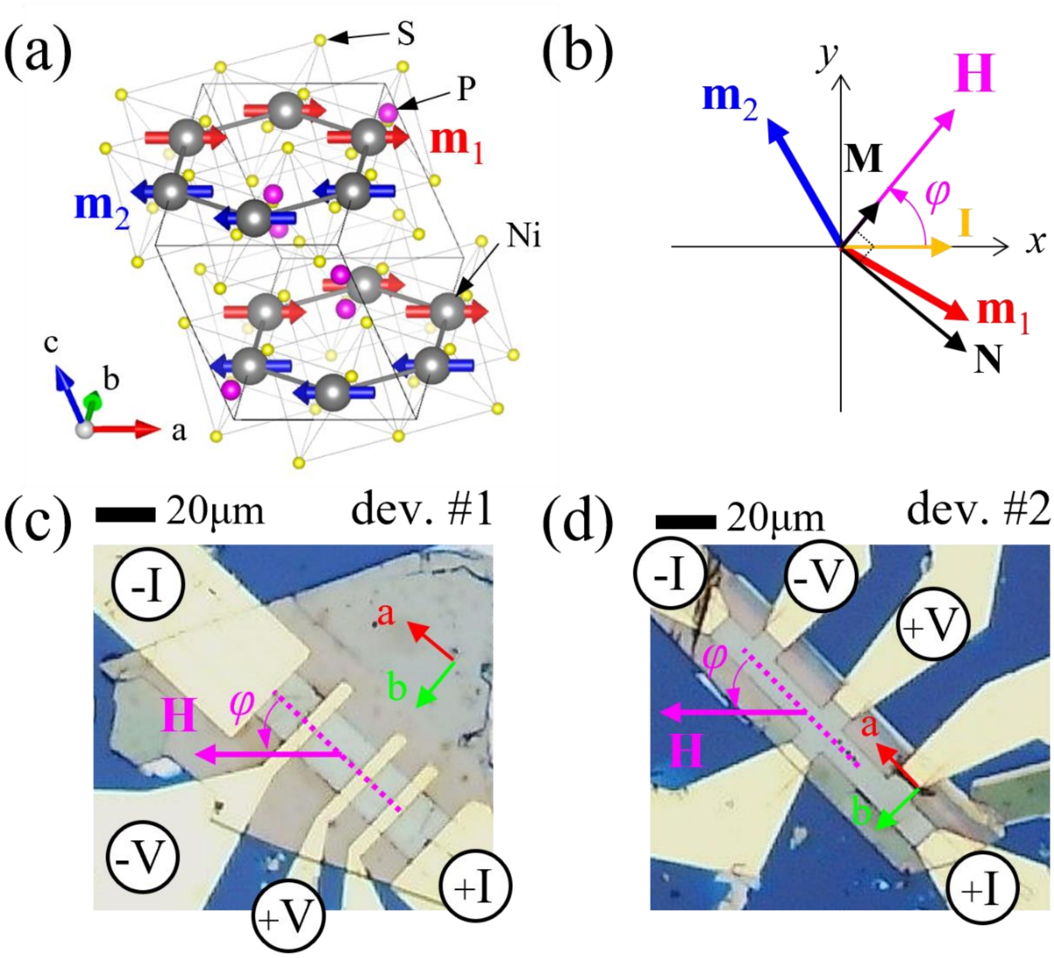

Figure 1 Sugi et al.

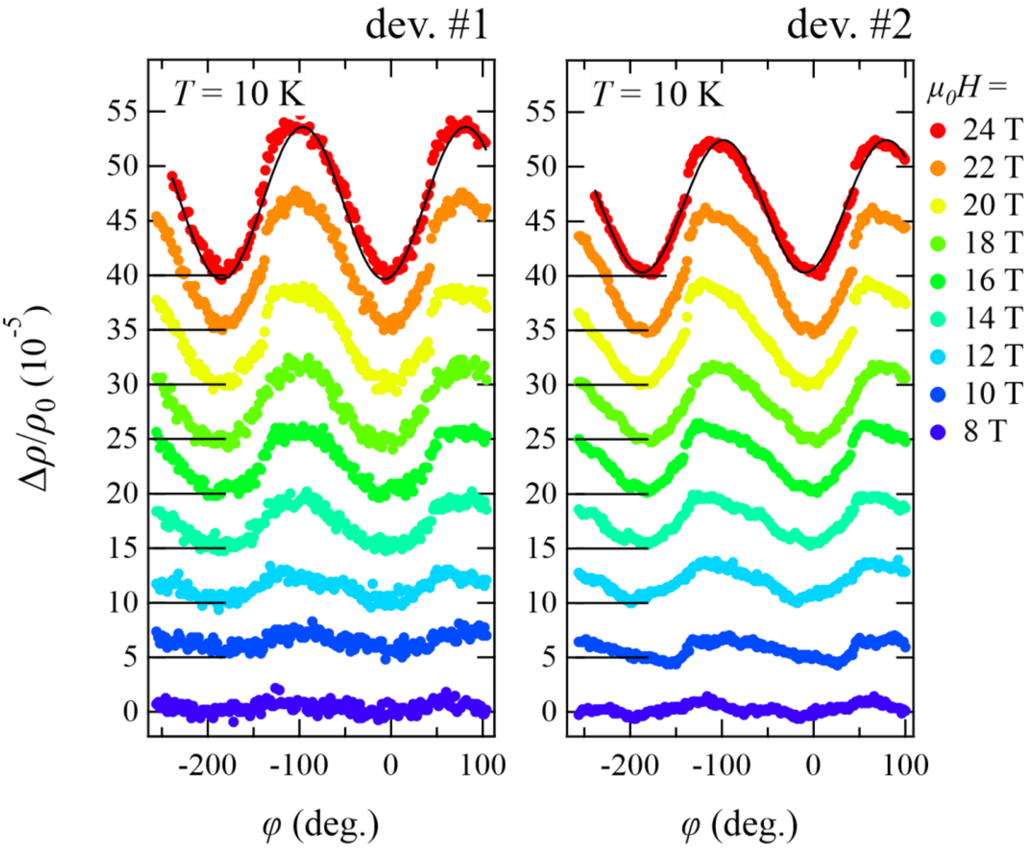

Figure 2 Sugi et al.

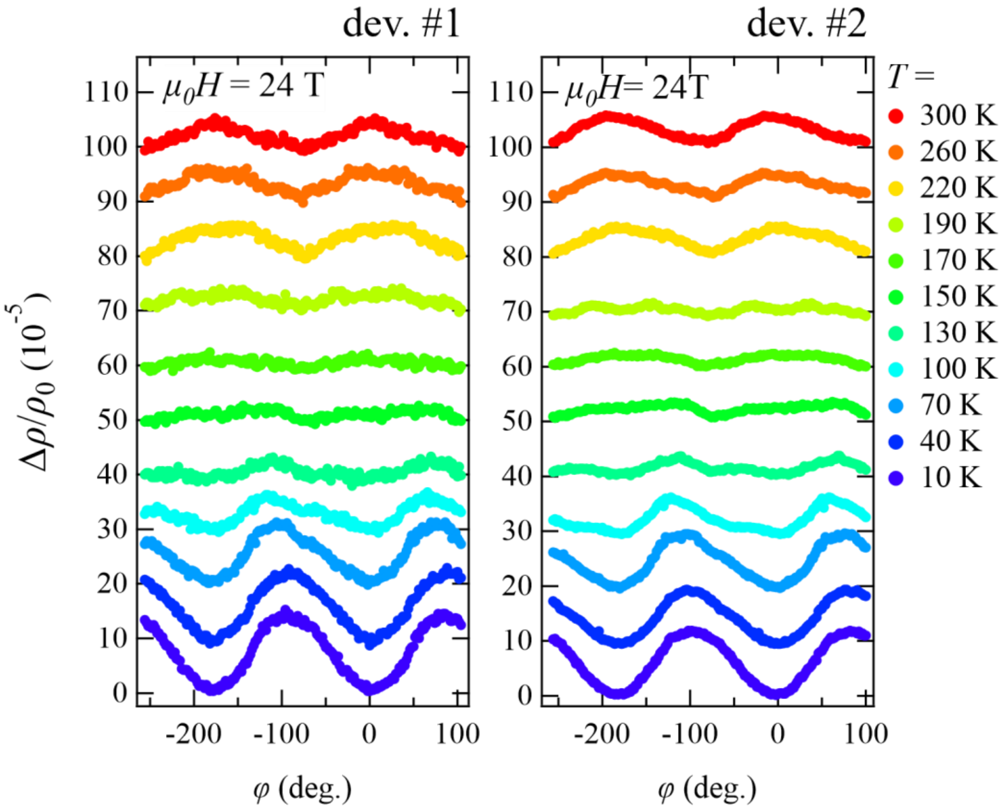

Figure 3 Sugi et al.

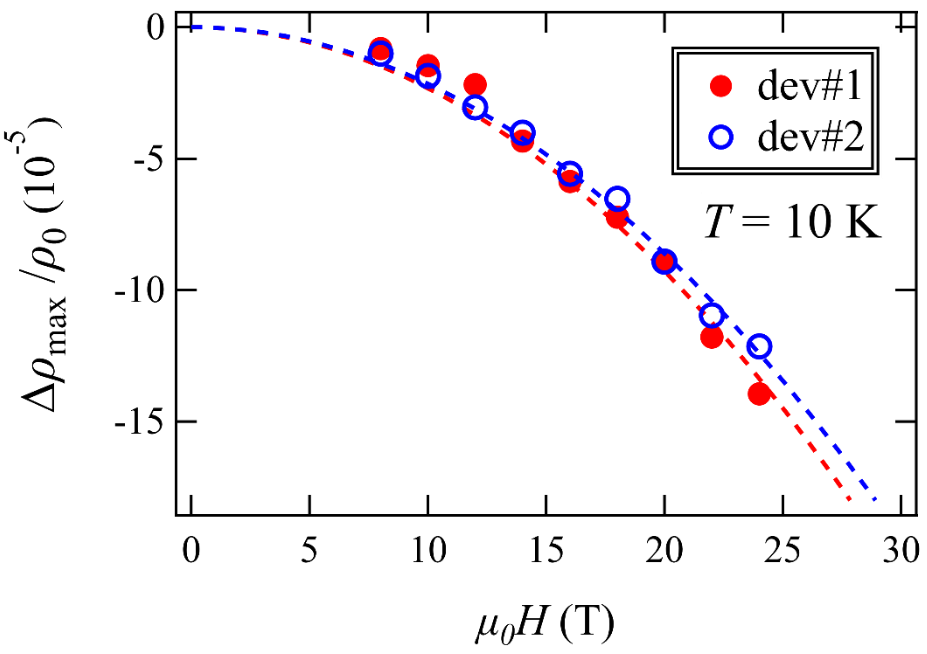

Figure 4 Sugi et al.

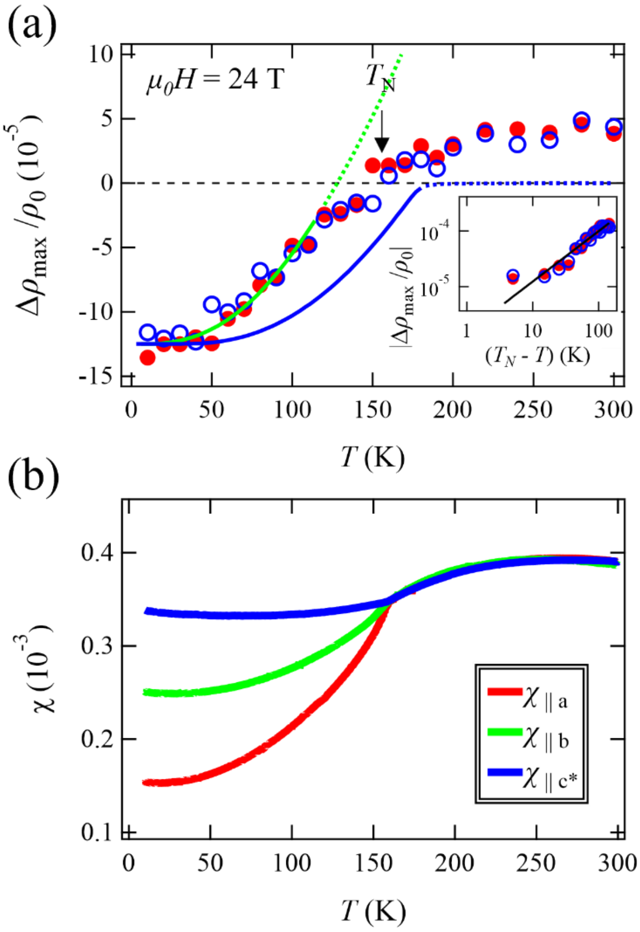

Figure 5 Sugi et al.

References:

[1] V. Baltz, A. Manchon, M. Tsoi, T. Moriyama, T. Ono, and Y. Tserkovnyak, Rev. Mod. Phys. **90**, 015005 (2018).
[2] T. Jungwirth, X. Marti, P. Wadley, and J. Wunderlich, Nat. Nanotechnol. **11**, 231 (2016).
[3] X. Marti, I. Fina, C. Frontera, J. Liu, P. Wadley, Q. He, R. J. Paull, J. D. Clarkson, J. Kudrnovský, I. Turek, J. Kuneš, D. Yi, J. H. Chu, C. T. Nelson, L. You, E. Arenholz, S. Salahuddin, J. Fontcuberta, T. Jungwirth, and R. Ramesh, *Nat. Mater.* **13**, 367 (2014).
[4] T. Moriyama, N. Matsuzaki, K. J. Kim, I. Suzuki, T. Taniyama, and T. Ono, *Appl. Phys. Lett.* **107**, 1 (2015).
[5] P. Wadley, B. Howells, J. Elezny, C. Andrews, V. Hills, R. P. Campion, V. Novak, K. Olejnik, F. Maccherozzi, S. S. Dhesi, S. Y. Martin, T. Wagner, J. Wunderlich, F. Freimuth, Y. Mokrousov, J. Kune, J. S. Chauhan, M. J. Grzybowski, A. W. Rushforth, K. W. Edmonds, B. L. Gallagher, and T. Jungwirth, *Science* **351**, 587 (2016).
[6] T. Moriyama, M. Kamiya, K. Oda, K. Tanaka, K. J. Kim, and T. Ono, *Phys. Rev. Lett*. **119**, 1 (2017).
[7] T. Moriyama, W. Zhou, T. Seki, K. Takanashi, and T. Ono, *Phys. Rev. Lett.* **121**, 167202 (2018).
[8] X. Z. Chen, R. Zarzuela, J. Zhang, C. Song, X. F. Zhou, G. Y. Shi, F. Li, H. A. Zhou, W. J. Jiang, F. Pan, and Y. Tserkovnyak, *Phys. Rev. Lett*. **120**, 1 (2018).
[9] T. Moriyama, K. Oda, T. Ohkochi, M. Kimata, and T. Ono, *Sci. Rep.* **8**, 1 (2018).
[10] H. Wang, C. Du, P. C. Hammel, and F. Yang, *Phys. Rev. Lett.* **113,** 097202 (2014).
[11] T. Moriyama, S. Takei, M. Nagata, Y. Yoshimura, N. Matsuzaki, T. Terashima, Y. Tserkovnyak, and T. Ono, *Appl. Phys. Lett.* **106,** 162406 (2015).
[12] C. Hahn, G. Loubens, V. V. Naletov, J. B. Youssef, O. Klein, and M. Viret, *Europhys. Lett.* **108,** 57005 (2014).
[13] R. Lebrun, A. Ross, S. A. Bender, A. Qaiumzadeh, L. Baldrati, J. Cramer, A. Brataas, R. A. Duine and M. Kläui, Nature 561, 222 (2018).
[14] J. Li, C. Blake Wilson, R. Cheng, M. Lohmann, M. Kavand, W. Yuan, M. Aldosary, N. Agladze, P. Wei, M. S. Sherwin, and J. Shi, Nature 578, 70 (2020).
[15] P. Vaidya, S. A. Morley, J. van Tol, Y. Liu, R. Cheng, A. Brataas, D. Lederman, E. del Barco, Science 368, 160 (2020).
[16] T.Moriyama, K. Hayashi, K. Yamada, M. Shima, Y. Ohya, Y. Tserkovnyak, and T. Ono, Physical Review B 101, 060402 (2020).
[17] F. Feringa, G. E. W. Bauer and B. J. van Wees, ArXiv:2201.13241 (2022).
[18] R. Wu, A. Ross, S. Ding, Y. Peng, F. He, Y. Ren, R. Lebrun, Y. Wu, Z. Wang, J. Yang, A. Brataas and M. Kläui, ArXiv: 2112.07306 (2021).
[19] *R. Brec, D. M. Schleich, G. Ouvrard, A. Louisy, J. Rouxel, Inorg. Chem. 1979, 18, 1814.*
[20] P. A. Joy and S. Vasudevan, Phys. Rev. B 46, 5425 (1992).
[21] K. Kurosawa, S. Saito, and Y. Yamaguchi, J. Phys. Soc. Jpn., 52, 3919 (1983).
[22] A. R. Wildes, V. Simonet, E. Ressouche, G. J. McIntyre, M. Avdeev, E. Suard, S. A. J. Kimber, D. Lançon, G. Pepe, B. Moubaraki and T. J. Hicks, *Phys. Rev. B* **92**, 224408 (2015).
[23] E. B. Sonin Adv. Phys. 59, 181 (2010).
[24] G. R. Hoogeboom, A. Aqeel, T. Kuschel, T. T. M. Palstra, and B. J. van Wees, *Appl. Phys. Lett.* **111**,052409 (2017).
[25] L. Baldrati, A. Ross, T. Niizeki, C. Schneider, R. Ramos, J. Cramer, O. Gomonay, M. Filianina, T. Savchenko, D. Heinze, A. Kleibert, E. Saitoh, J. Sinova, and M. Kläui, *Phys. Rev. B* **98**, 1 (2018).
[26] Y. Ji, J. Miao, K. K. Meng, Z. Y. Ren, B. W. Dong, X. G. Xu, Y. Wu, and Y. Jiang, *Appl. Phys. Lett.* **110**, 262401 (2017).
[27] R. Schlitz, T. Kosub, A. Thomas, S. Fabretti, K. Nielsch, D. Makarov, and S. T. B. Goennenwein, *Appl. Phys. Lett.* **112**, (2018).
[28] K. Oda, T. Moriyama, M. Kimata, S. Kasukawa and T. Ono, *Jpn. J. Appl. Phys.* **59**, 010908 (2020).
[29] H. Nakayama, M. Althammer, Y.-T. Chen, K. Uchida, Y. Kajiwara, D. Kikuchi, T. Ohtani, S. Geprags, M. Opel, S. Takahashi, R. Gross, G. E. W. Bauer, S. T. B. Goennenwein, and E. Saitoh, Phys. Rev. Lett. **110**, 206601 (2013).

[30] Y-T. Chen, S. Takahashi, H. Nakayama, M. Althammer, S. T. B. Goennenwein, E. Saitoh, and G. E. W. Bauer, Phys. Rev. B 87, 144411 (2013).

[31] J. Fischer, O. Gomonay, R. Schlitz, K. Ganzhorn, N. Vlietstra, M. Althammer, H. Huebl, M. Opel, R. Gross, S. T. B. Goennenwein and S. Geprägs, *Phys. Rev. B* **97**, 014417 (2018).

[32] M.-H. Nguyen, D. C. Ralph, and R. A. Buhrman, Phys. Rev. Lett. **116**, 126601 (2016).

[33] S. Vélez, V. N. Golovach, A. Bedoya-Pinto, M. Isasa, E. Sagasta, M. Abadia, C. Rogero, L. E. Hueso, F. S. Bergeret, and F. Casanova, Phys. Rev. Lett. **116,** 016603 (2016).

[34] T. Kato, Y. Ohnuma, and M. Matsuo, Phys. Rev. B **102**, 094437 (2020).

[35] See the Supplemental Material at URL, which includes Refs. [36-37], for theoretical development.

[36] T. Kato, Y. Ohnuma, and M. Matsuo, Phys. Rev. B 102, 094437 (2020).

[37] D. Lancon, R. A. Ewings, T. Guidi, F. Formisano, and A. R. Wildes, Phys. Rev. B **98**, 134414 (2018).